Mechanical, tribological and fractography analysis of structural grade Al7075/n-TiC composites and optimization of wire EDM parameters through Taguchi method

Ravikumar M, Chidanand Kishor Mangrulkar
Dept., of Mechanical Engineering, B M S College of Engineering, Karnataka, India
ravikumarm.mech@bmsce.ac.in, https://orcid.org/0000-0002-4958-839X
chidanandkm.mech@bmsce.ac.in

Vinod B R
Department of Civil Engineering, B.M.S Institute of Technology and Management, Bengaluru -560119, KA, India
vinod.vbr@gmail.com

Balaji Y S
Department of Mechanical Engineering, Nagarjuna College of Engineering and Technology, Bangalore, KA, India
ys.balaji@gmail.com

Hemaraju
Department of Mechanical Engineering, B G S Institute of Technology, Adichunchanagiri University, B G Nagar, Nagamangala (T), Mandya (D), KA, India
hemaraju@bgsit.ac.in

ABSTRACT. The effects of nanoscale TiC (n-TiC) reinforcement on Al7075 composites made by stir casting with 0%, 1%, 2%, 3%, and 4% reinforcement are examined in this work. The existence of n-TiC particles in the aluminum matrix was verified by microstructural investigation. When compared to un-reinforced alloy (Al7075), the mechanical, tribological, and wear properties were greatly improved by the addition of n-TiC; hardness, tensile strength, and wear resistance increased by 28.57%, 24.41%, and 33.69%, respectively. Molybdenum wire was used as the electrode material in an experimental investigation of the produced nano composites' machinability characteristics during Wire Electrical Discharge Machining (WEDM). Two machining attributes, Material Removal Rate (MRR) and Surface Roughness (SR), are

Citation: Ravikumar, M., Mangrulkar, C. K., Vinod, B R., Balaji, Y S., Hemaraju., Mechanical, tribological and fractography analysis of structural grade Al7075/n-TiC composites and optimization of wire EDM parameters through Taguchi method, Fracture and Structural Integrity, 77 (2026) 421-436.

Received: 06.03.2026
Accepted: 18.05.2026
Published: 14.06.2026
Issue: 07.2026

examined in connection to the combinational values of pulse time ON, pause time OFF, as well as peak current, which are chosen as the changeable input process elements. The results of the experiment showed that as pulse on time and peak current levels increased, so did MRR and Ra values. Under these circumstances, the wire electrode has maximum current, which makes it simple to remove more material and produce a moderate surface finish. The ANOVA results show that the "Pulse ON Time" has the biggest impact (47.01 %) on MRR and 36.64% impact on surface roughness values compared to the other factors, making it the most important parameter. The confirmatory test results revealed that the errors in MRR and Ra values were within acceptable limits. In the present research work, Taguchi methods have been successfully implemented to identify the optimum machining conditions for Al7075/n-TiC composites.

KEYWORDS. Al7075, n-TiC, Micro-structure, Mechanical, Wear, Fracture Surface, Wire EDM, Taguchi.

INTRODUCTION

Composite materials have appeared as a vital class of engineering materials owing to their superior combination of mechanical, tribological, thermal, properties compared to conventional monolithic materials. They are ideal for sophisticated structural and dynamic applications due to their high strength-to-weight ratio, superior fatigue resistance, and enhanced corrosion and wear properties. These benefits have led to the widespread use of composite materials in vital components such drive-shafts, engine rotors, armored vehicles, engine parts, and small bicycle frames [1]. Furthermore, metal matrix composites (MMCs) have become widely accepted in industry, especially in the automotive and aerospace sectors. To improve performance and fuel efficiency, top manufacturers like Honda, Toyota, General Motors, and Nissan use MMCs in engine blocks, piston rings, brake calipers, and connecting rods [1, 2]. Aluminum and its alloys are the most popular matrix materials for MMC construction because of their great compatibility with a variety of reinforcements, low density, superior castability, and high specific strength. Aluminum oxide (Al_2O_3), silicon carbide (SiC), boron carbide (B_4C), titanium carbide (TiC), and boron nitride (BN) are examples of ceramic reinforcements that can be applied to aluminum matrix composites (AMCs) to obtain desired mechanical and tribological properties [2,3]. AMCs are perfect for demanding applications in the automotive, electronic packing, aerospace, and defense industries because these reinforcements significantly boost the base alloy's hardness, mechanical stiffness, wear resistance, and load-bearing capability [3]. The focus has recently shifted from micro-scale reinforcements for nano-scale reinforcements due to their greater strengthening efficiency. Even at relatively low weight fractions, nanoparticles provide significant mechanical and tribological advantages over conventional micro-sized particles. This increase is mostly due to their significant surface area-to-volume ratio, which encourages improved interfacial bonding and effective load transfer among the matrix and reinforcement [2]. Additionally, nanoparticles act as nucleation sites during solidification, refining the grain and producing a more homogeneous microstructure. Additionally, by stopping dislocation motion within the matrix, they enhance hardness, tensile strength, as well as wear resistance [4]. However, despite these advantages, issues such poor wettability, uneven dispersion at higher reinforcement's levels, and particle agglomeration remain limit their effectiveness and necessitate further study. Many manufacturing processes, such as liquid-state processing, vapor evaporation, and powder metallurgy, have been developed for the fabrication of MMCs. Stir casting is one of the most widely used of them due to its price, convenience of usage, and adaptability for large-scale manufacture [5]. Prior to solidification, stir casting entails adding strengthening particles to the molten metal as well as distributing them uniformly through mechanical stirring. The final microstructure and characteristics of the composite are greatly influenced by process variables such as temperature, stirring speed, as well as particle addition technique. These properties need to be carefully managed in order to achieve uniform particle dispersion and minimize defects like porosity and clustering. Despite considerable advancements in MMC research, these materials are very challenging to machine because to the presence of abrasive and rough reinforcing particles. Reduced dimensional accuracy, poor surface polish, and rapid tool wear might result from conventional machining methods. To overcome these limitations, non-traditional machining techniques like Wire Electrical Discharge

Machining (WEDM) have grown to be more popular. WEDM is perfect for precisely machining complex and hard materials under low mechanical stresses since it is a thermo-electric technology that uses controlled electrical discharges to eliminate material. Optimizing machining parameters is crucial to achieving desired performance attributes such low Surface Roughness (Ra) and high Material Removal Rate (MRR). Statistical and optimization techniques such as Response Surface Methodology (RSM) as well as Taguchi methods are often used to systematically analyze the impact of process parameters and identify optimal machining settings [6]. RSM may effectively improve WEDM parameters for machining steel and titanium alloys, enhancing surface integrity and machining efficiency, according to earlier studies [6–8]. Taguchi-based techniques combined with Analysis of Variance (ANOVA) are being effectively used to determine the significance of process elements and their interactions. Although aluminum-based composites as well their machining behavior have been thoroughly studied, there is a substantial research gap in the comprehensive analysis of nano TiC (n-TiC) reinforced Al7075 composites, particularly with regard to the combined assessment of microstructural features, mechanical properties, wear behavior, and machinability. TiC and other nanoscale reinforcements can enhance the performance of Al7075, a high-strength aluminum alloy that is commonly used in aerospace and defense applications. Few studies have examined the synergistic impact of n-TiC addition on material properties and machining performance, especially those that employ integrated experiential and statistical approaches. Furthermore, most existing research focuses on either material development as well as machining optimization independently, failing to make a clear link between the increased material qualities and their machinability aspects. This absence of integrated analysis limits the practical utility of such research in real production environments. By developing Al7075/n-TiC nano-composites using the stir casting technique and methodically examining their microstructural, mechanical, and tribological characteristics, the current study seeks to close these gaps. Additionally, WEDM is used to assess the created composites' machinability, and the Taguchi approach in combination with ANOVA is used to improve the process parameters. Investigating the impact of n-TiC reinforcements on the microstructure, mechanical, wear, and machinability properties of Al7075 nano composites is the innovative aspect of the study project. The machinability properties of MRR and surface roughness during the machining of produced micro MMCs were assessed using Taguchi and ANOVA. Studying the improvement of material properties through machining process optimization is a novel method.

METHODS USED IN THE EXPERIMENT

Method of composites fabrication

Electric furnace was utilized to heat brilliant extruded rod made of aluminum alloy (Al7075). To fully melt the alloy, it was heated to between 650°C and 750°C. For this investigation, n-TiC hard ceramic particles that were likewise warmed were used as reinforcement. The molten aluminum alloy was combined with the heated ceramic particles, and the mixture was constantly agitated. The uniform dispersion of particles in the Al alloy matrix materials is guaranteed by the stirring procedure. Afterwards, the temperature of the melt containing the Al alloy combination and the reinforcing particles was kept at 700 ± 10°C. Thereafter, the melt was placed into a metallic mold box that measured 150mm * 150mm * 10mm for specimen preparation. In the present research work, the weight percentage of nano sized TiC was varied from 0 - 4% in steps of 1 %.

Microstructure analysis

To achieve a smooth, mirror-like surface appropriate for microstructural and SEM investigation, the specimens were mechanically ground using various grades of emery sheets (up to 1200 grit), polished with diamond suspensions, and then finished with 1 μm diamond suspension. After being exposed to Keller's reagent, the samples were thoroughly cleaned using a sterile towel. The ASTM B483 standards were followed in conducting the analysis. Following etching and air drying, SEM examination was done to examine the microstructure of the as-cast and redmud nanoparticle-reinforced specimens.

Hardness test

A computerized micro hardness testing device (FIE-VM:50 PC) was used to assess the micro-hardness of the produced nano-composite samples. Every composite sample was polished to a mirror finish in order to prepare it for microhardness testing. The polished surfaces on the nano composite were indented using a diamond tip indenter that weighs 100 grams and has a dwell period of 10 seconds during the measurement of hardness. Three microhardness measurements are performed on the sample, and the average results are shown together with error bars that show the highest and lowest values. The sample preparations as well as testing were performed as per ASTM E-92 standards.

Tensile test

The experiments were conducted using a calibrated universal testing machine (UTM) with a maximum load capacity of 450 kN, which is capable of accommodating high-strength materials and providing precise measurements of load and displacement. During the test, ultimate tensile strength was recorded until specimen failure occurred. Tensile testing of the prepared specimens was carried out in accordance with the standardized procedures outlined in ASTM E8, ensuring accuracy and reproducibility of results.

Wear test

Wear testing was conducted in according to ASTM G99 standards. A 10 N load, a 500 rpm sliding speed, as well as a total distance of sliding of 1000 meters were applied to test the samples by sliding them over an EN-32 grade steel disc. In compliance with ASTM G99-05, the test specimens were prepared with the dimensions of 6 mm in diameter as well as 30 mm in length. The wear properties of the as-cast and nano-composites specimens were assessed using the weight loss method. Each specimen was pressed up against the rotating hard steel disk during testing. The specimens were weighed again after each test, and the wear rate was determined by comparing the initial and final weights.

Machinability test

WEDM method was used to cut the fabricated nano composites under several machining conditions, such as current, pulse time on, and pulse time off. Process parameter optimization was the main objective of the Taguchi process [7]. Based on the previously completed literature review, the main process variables, peak current (A), pulse time on (μS), as well as pulse time off (μS), were selected as parameters for the experimental work at different levels. Furthermore, during the trials, the n-TiC content did not change. Based on the mechanical and wear behavior of the produced nano composites, the sample with the best attributes was selected to study the machining characteristics, such as MRR and Ra. Cutting speed and kerf width were the response parameters used to evaluate the performance of the machining process. Tab. 1 lists the elements and its three levels considered for the experimental investigation. Material Removal Rate (MRR) was determined by dividing the amount of material removed by the machining time. Use the "Mitutoyo" Surface Roughness Tester was used after the machining was completed. Digital surface roughness values based on Ra, Rz, and Rq were computed using a probe that travels a predefined distance. A Mitutoyo surface roughness tester was used to assess the surface roughness (SR) of the produced nano composites. The numerical average-roughness (Ra) value was used to determine the SR of the machined samples. Ra is the average of three measurements of the material's surface roughness.

RESULTS AND DISCUSSION

Analysis of microstructure

Fig. 1 displays the optical microstructures of the fabricated composites. ASTM guidelines were followed for both sample preparation and testing. The microstructure of as-cast Al7075 is shown in Fig. 1(a). A typical cast Dendritic Arm Structure (DAS), which was formed as a result of the rapid cooling during solidification, makes up the majority of the microstructures. Fig. 1(b) indicates the presence of nano TiC particulates which is highlighted with the marking. It means presence of nano particulates with uniform distribution within the base material. When n-TiC particles are added, the dendritic arms typically thin out and produce new grains. However, Fig. 1(c) shows that the dendritic structural refinement is not particularly substantial at 4 weight percent n-TiC addition. Because of the components in Al7075, the DAS shows long α-Al dendritic arms covered in Al2CuMg and Al2Cu phases. The dendritic structure of the as-cast Al7075 has dissipated as a result of the multi-step casting and inclusion of n-TiC particles, which altered the solidification pattern. The microstructures show that the n-TiC particle and Al matrix have a fine interface and strong interfacial bonding. In order to support and transfer the applied load to the particles for improved mechanical and tribological properties, interfacial bonding is required. The correct wetting of n-TiC, which is the outcome of the stirring process and its parameters, is primarily responsible for the interfacial bonding that is attained. Additionally, as their content grows, n-TiC particles clump together to form larger particles, as shown by the yellow color mark. Nevertheless, the later phases become coarser and no discernible refinement is seen until 3 weight percent of n-TiC is added. The multi-step stirring method employed in this study enhances wetting, eliminates reinforced particle clumping, and evenly distributes the particles throughout the melt. Because the stirring is done in many steps, the gas layers on the particles are immediately split, increasing the wetting angle and reducing shrinkage and particle clustering. The distribution of n-TiC in the matrix is also influenced by variations in the densities of the n-TiC Al matrix [8].

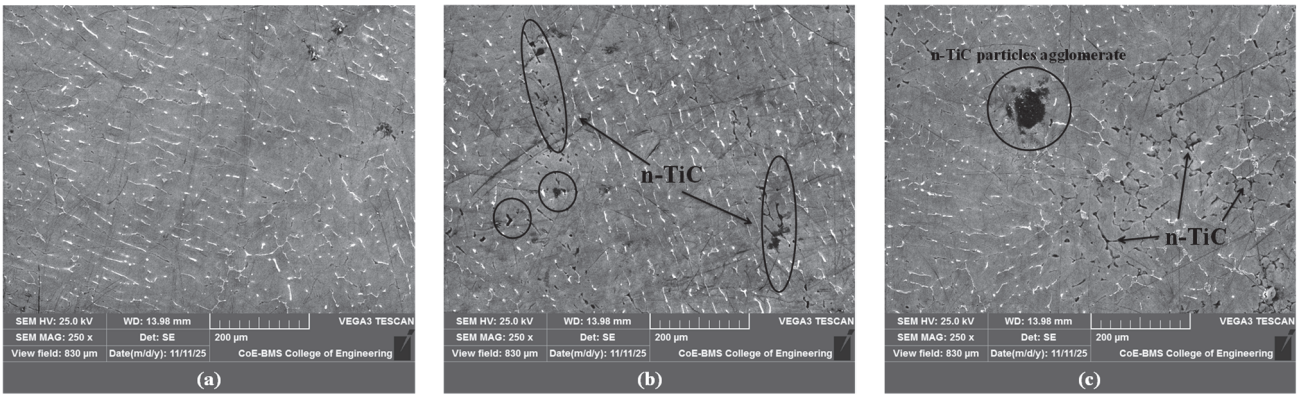

Figure 1: Micro-structure of (a) matrix (Al7075), (b) Al7075 + 3 % of n-TiC and (C) Al7075 + 4 % of n-TiC

Hardness analysis

The developed nano MMCs' hardness values are displayed on Fig. 2. The microhardness of the composites was shown to progressively rise as the amount of n-TiC added increased. When compared to the unreinforced Al7075 sample, the composite sample with up to 3 weight percent n-TiC particles showed a maximum hardness of 91 VHN, which is 28.57% higher. Since n-TiC particles are more resistant to plastic deformation than Al7075, their hardness is significantly higher. Grain size reduction, which results in greater grain boundaries, is another factor that affects hardness. The n-TiC particles produce heterogeneous nucleation in the matrix by acting as nucleating agents. Consequently, nucleation sites increase as the weight percentage of n-TiC increases, leading to matrix microstructure refinement. Grain boundaries increase with increasing grain fineness. According to the Hall-Petch relation [8], these grain boundaries obstruct the slip planes and cause raise in the hardness. Additionally, it was shown that the hardness of the produced nano MMCs decreased with 4 weight percent addition of n-TiC. The main cause of the reduction in hardness of nanocomposites at greater weight percentages of nano-reinforcements is particle agglomeration, or clustering, which results in weak spots, encourages flaws, increases porosity, and obstructs efficient load transfer from the matrix to the particles. Excess particles result in poor dispersion and interfacial bonding, whereas low reinforcing levels enhance characteristics. Because of their high surface energy, nanoparticles tend to cluster together rather than disperse uniformly as reinforcement an increase, which lower the effective reinforcement surface area and creates stress concentration regions. The material's resistance to indentation may be diminished by large clusters, which may function as flaws rather than strengthening agents.

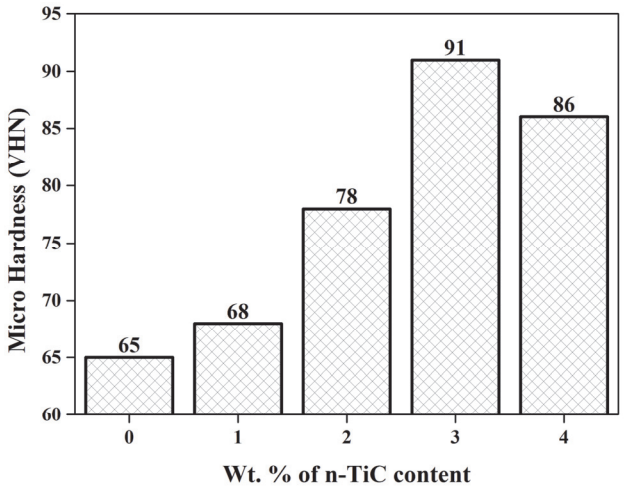

Figure 2: Micro-hardness of nano-composites.

Tensile test analysis

Fig. 3 (a) displays the UTS variation of n-TiC reinforced Al7075. The tensile strength of the fabricated nano composites was higher than that of the unreinforced Al7075. The nano composites have demonstrated a considerable amount of plastic strain prior to fracture, indicating a good work hardening capacity. In comparison to the unreinforced Al7075, the fabricated nano composite with 3 weight percent n-TiC is found to demonstrate maximum strength with UTS of 172

MPa, which is 24.41 percent greater. Because n-TiC ceramic particles are harder than the basic alloy, their addition has strengthened the composites. Through both direct and indirect strengthening mechanisms, the reinforcement has given the composites more strength. Direct strengthening, which directly affects load transfer, is based on strong interfacial adhesion between the matrix as well as nano reinforcement. Additionally, interfacial bonding influences the presence of pores, microcracks, and microvoids as well as the wetting angle among the matrix and nano-reinforcement. A uniform distribution of the hard particles directly influences the tensile strength for composites in the present study. The main focus of secondary strengthening is how reinforcement affects the matrix phase. The enhanced strength of the resulting composites was due to the following strengthening mechanisms [9]: (1) Grain refinement; (2) dispersion strengthening caused by n-TiC particles; (3) tension between the matrix as well as nano reinforcement, etc. Usually, these factors complement each other. As previously stated, particles that are dispersed in the matrix cause these dislocations to move when a force is applied to the material, forming dislocation loops or bows surrounding the particle that function as a barrier to its movement and improve the strength. Next, grain refining produces smaller grains and more grain boundaries that restrict dislocation motion, in accordance with Hall-Petch theory [10]. Additionally, the results show that at 3 weight percent addition, the phases get coarser and the n-TiC particles tend to agglomerate. Instead of serving as reinforcements, these clusters concentrate stress, which lowers the total tensile strength. Additionally, achieving uniform dispersion is challenging with higher loading. Inadequate contact or inadequate adhesion among the particulates and the matrix cause premature failure. It can also be argued that an excessive number of nanoparticles cause the mixture to become more viscous, which leads to poor wettability, and the formation of voids, all of which significantly weaken the material [11]. Fig. 3 (b) shows the engineering curves of stress and of the basic alloy as well as the composites reinforced with various weight percentages of nano-TiC (n-TiC). The graphs illustrate how ceramic nanoparticle reinforcement affects the matrix alloy's strength, ductility, as well as tensile deformation behavior. As is typical of ductile metallic materials, the base alloy shows the lowest tensile strength but relatively higher elongation. A notable increase in tensile strength is seen with the addition of n-TiC particles. The composite with 3 % n-TiC content exhibits the best ultimate tensile strength (UTS), whereas a 4 % addition causes a minor decrease in strength and ductility. This behavior shows that there is an ideal concentration of reinforcement for efficient load transfer and strengthening. Hooke's law states that stress is directly proportional to strain in the elastic deformation region, which is represented by the first linear section of the curves. This region's slope indicates the material's elastic modulus. Following yielding, dislocation multiplication and interaction cause plastic deformation, which is followed by strain hardening. Effective resistance to plastic deformation is indicated by the slow rise in stress upon yielding. The composite reinforced with 3 % n-TiC has the highest ductility and strength combination, indicating effective interfacial bonding and homogeneous particle dispersion. Nevertheless, a decrease in tensile performance is noted at 4 % n-TiC. Particle agglomeration, poor wettability, and stress concentration effects, which encourage early crack initiation and propagation, could be the cause of this. Because stiff particles limit plastic movement and diminish matrix continuity, excessive ceramic reinforcing typically reduces ductility. The beginning of necking and the accumulation of damage before fracture are correlated with the decreasing stress after achieving the peak stress. The switch from flexible to somewhat brittle behavior caused by the presence of hard ceramic particles is confirmed by the decrease in elongation with increasing reinforcement content. Overall, the stress-strain behavior demonstrates that adding the ideal quantity of n-TiC reinforcement greatly improves the alloy's mechanical performance through a combination of strengthening methods while preserving adequate ductility.

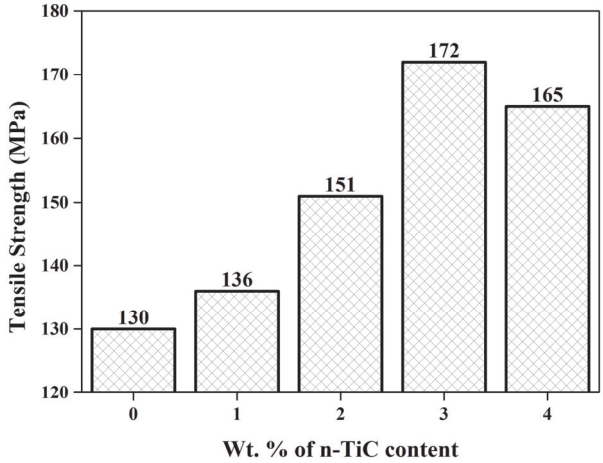

Figure 3 (a): Tensile strength of nano-composites.

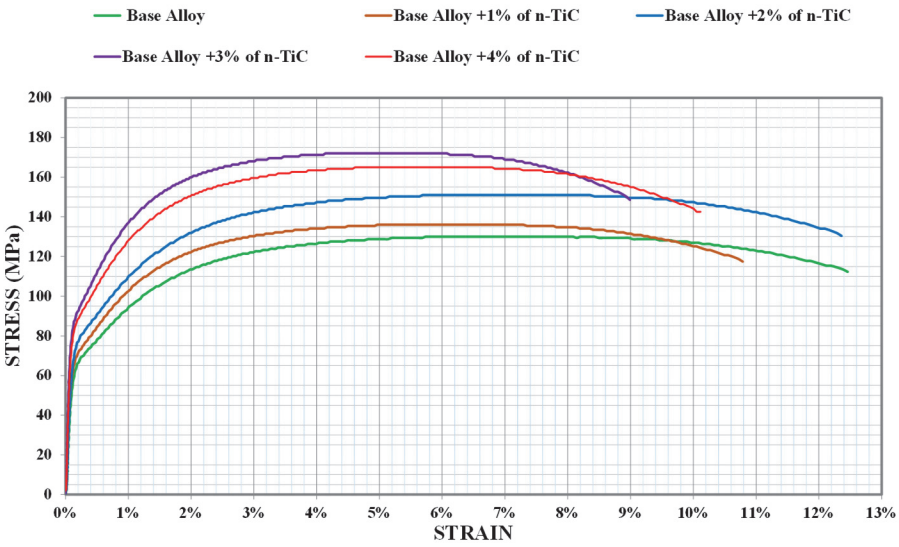

Figure 3 (b): Stress strain curve for the developed nano-composites.

The tensile specimen's SEM and fractography studies are displayed in Fig. 4. For composites with varying weight percentages of n-TiC particles, fracture surface characterization showed distinct topographies. Large dimples and significant plastic deformation were found in the fracture surface analysis of fracture toughness specimens of Al7075 alloy samples, indicating a ductile fracture. As seen in Fig. 4(a), the fracture surfaces also display shallow, fine dimples that suggest the fracture is ductile. Because there were too many n-TiC particles present, the fracture surface of nano-MMCs with 3% mass fraction nano reinforcement showed a cleavage type of fracture (Fig. 4(c)). Additionally, regions of clustered particles for reinforcement exceeding 3% of mass fractions (Fig. 4(b)) are susceptible to early damage in the composites, and the large particles appear to be more likely to fracture, which is why the fracture-toughness value decreased. Micro-crack nucleation and propagation dominated the matrix alloy's fracture mode, which shifted from ductile to cleavage type (in the case of nano-MMCs). Observations of MMCs under a scanning electron microscope indicate that void nucleation may occur at large participants in addition to the matrix/nano-particle interface at higher reinforcement content (4% of mass fractions, Fig. 4(c)). At lower reinforcement rates, the fracture appears to occur through the breakage of the nano-particles. Lastly, cleavage was seen in a nano-composite with 4% mass fraction dispersoids, suggesting a brittle fracture.

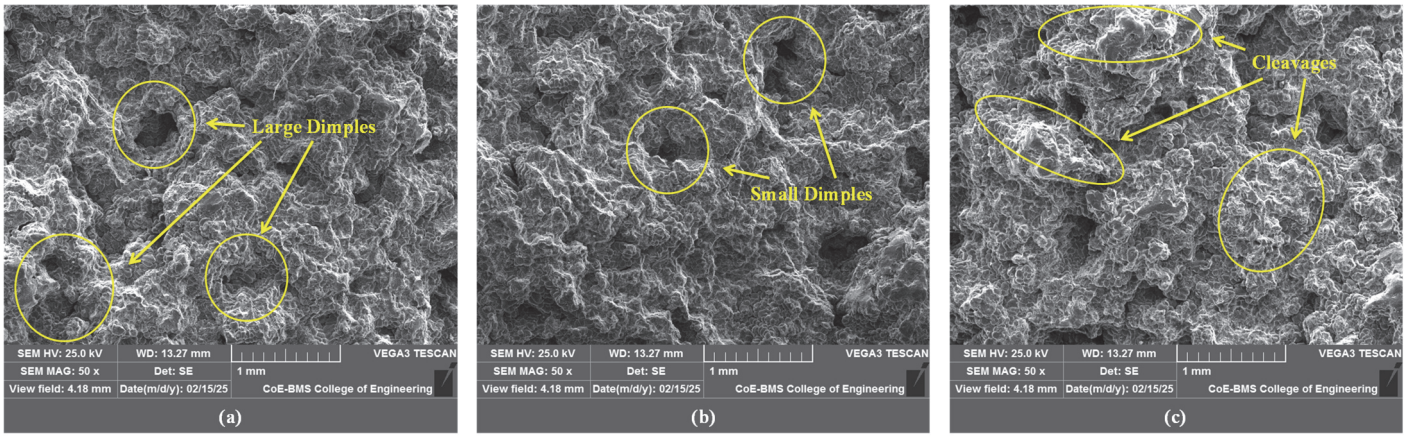

Figure 4: Fractured surface of (a) base alloy (Al7075), (b) composite with 3 % of n-TiC and (C) composite with 4 % of n-TiC

Wear test analysis

Fig. 5 illustrates how the fabricated nano composites' wear rate varies. It is evident that base alloy (Al7075) exhibited the highest wear rate when compared to n-TiC reinforced Al7075 composites. The concentrations of the reinforcing nanoparticles have a significant impact on the wear rate of Al/n-TiC nanocomposites. Because of the bindings at the

interfaces between the reinforcing nanoparticles and the aluminum alloy, the weight percentage of hard nano particulates increases wear resistance and decreases wear rate [1]. This is because the melting points of the aluminum alloy and the reinforcing nanoparticles differ, which causes thermal stresses at these interfaces that increase the interlocking dislocations [5]. The reinforcing nanoparticle improves wear resistance (lowering wear rate) and prevents dislocations from moving. Additionally, it is noted that the wear rate increased with larger weight percentages of n-TiC due to a number of reasons, including wettability and the bonding among the base metal and the nano-reinforcement [3]. These factors may cause the nano-composite's wear resistance to decline.

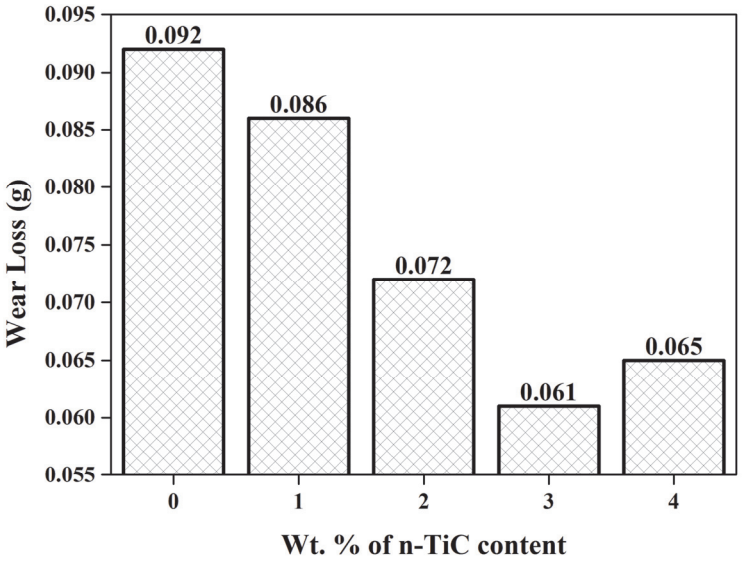

Figure 5: Wear loss of nano-composites.

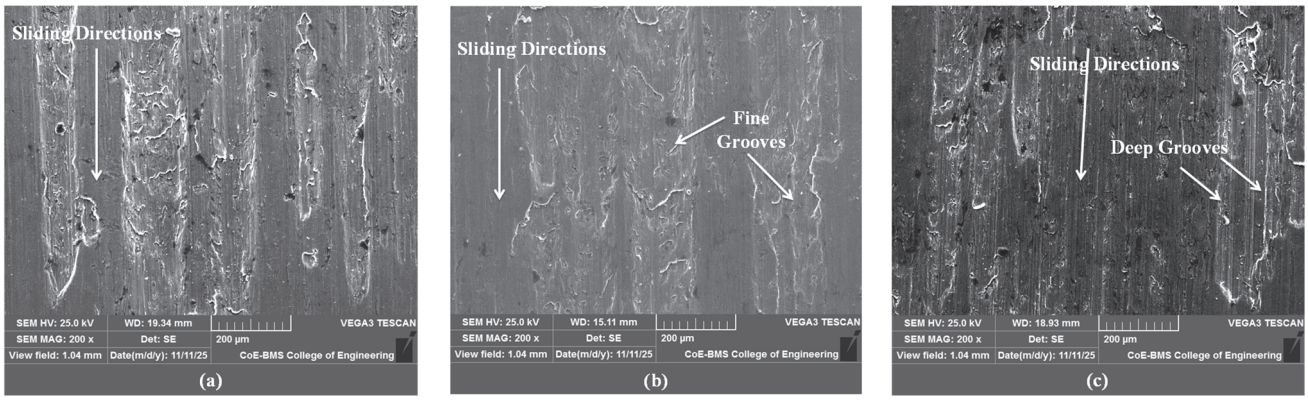

Figure 6: Wornout surface of (a) base alloy (Al7075), (b) composite with 3 % of n-TiC and (c) composite with 4 % of n-TiC.

The scanning electron microscopy analysis of the worn surface morphology of Al7075 samples and manufactured nano composites is shown in Fig. 6. When compared to the worn surface of the pure alloy, the surface morphology of aluminum alloy with nano TiC reinforcement shows some variations. Scratches and limited grooves were observed on the worn surface. These are unmistakable signs of hard particle abrasion. Because of the higher TiC content, the worn surface of the Al7075/3 weight percent n-TiC composite shows less wear and finer abrasion grooves, showing improved wear resistance [11]. Wear is decreased as a result of the improved load distribution provided by the higher reinforcing content. The increased n-TiC content reduces extreme wear and damage by reducing mechanical and thermal loads. In general, the composites' wear resistance rises as the TiC content does [12]. The wear behavior of the composite significantly alters when the reinforcing weight percentage surpasses the ideal threshold. SEM micrographs usually show mild abrasive wear with shallow, tiny scratches on the worn surface at lower or ideal reinforcing levels. This suggests reasonably good wear resistance and regulated material removal. Nevertheless, the wear mechanism changes to severe wear beyond the ideal reinforcing content. SEM pictures of the 4% n-TiC sample reveal significant surface degradation, deep grooves, and huge delamination pits. Increased fracture initiation and propagation as a result of particle aggregation and weaker matrix-

reinforcement bonding are suggested by this transition. Therefore, adding excessive reinforcement eventually results in poor wear resistance rather than enhancing the performance of the composite [10].

Optimization of wire EDM parameters

The material removal rate (MRR) as well as surface roughness (Ra) during WEDM machining were further examined using a 3% nano-TiC reinforced Al7075 composite. The results show that adding 3% nanoparticle improves mechanical characteristics and increases wear resistance. According to this context, the authors decided to investigate the 3% reinforced nano-composites further. A CONCORD WIRE DK7720 WEDM machine with a 0.18 mm diameter molybdenum wire electrode with deionized water as the dielectric medium was used to conduct the experiments. A schematic of the WEDM equipment is shown in Fig. 7. To guarantee stability while minimizing vibration during cutting, the workpiece was firmly secured on the machine table. Molybdenum wire was chosen for wire-cut EDM procedures because of its excellent electrical conductivity, high tensile strength, and repeated reusability. In order to remove material through localized melting and vaporization, regulated electrical discharges were created between the conductive workpiece and a continuously moving wire electrode during machining. To examine their impact on metrics for performance including material removal rate (MRR) and surface roughness (Ra), the machining parameters such as pulse-on time, pulse-off time, peak current, and wire feed rate were carefully set and modified in accordance with the experimental design. Continuous circulation of deionized fluid served as a cooler and dielectric medium in the machining zone. It aided in the manufacturing of sparks, removed eroded debris, as well as preserved dimensional precision and thermal stability. In order to avoid wire breakage and guarantee reliable cutting performance, proper cleaning pressure and wire tension have also been maintained. The input process characteristics were modified for each machining trial, and the ranges between them were selected based on previous studies and tests. The wire EDM factors for the procedure and the levels used in the present research are shown in Tab. 1. Response Surface Methodology (RSM) was used to examine the relationship among peak current (A), pulse time on (μS), and pulse time off (μS), with MRR and Ra values acting as the main response. Factorial designs for experiments are commonly employed to examine correlations between factors as well as responses under the assumption of linearity. In investigations where several process parameters combine in a non-linear way, as is typical in WEDM machining, DOE is especially helpful. DOE allows for the simultaneous examination of several input factors and their interactions, as opposed to changing one factor at a time. This makes it possible to identify both linear and non-linear correlations among variables and responses. This method saves time and money by drastically reducing the number of the experimental trials needed while yet yielding thorough and statistically sound results. The experimental design, which consists of 27 trials with various parameter combinations, is shown in Tab. 2.

Figure 7: Wire EDM equipment and setup.

Variables & Levels	Pulse ON Time (μs)	Pulse OFF Time (μs)	Current (Amp)
Level -1	20	9	3
Level 0	35	12	4
Level +1	50	15	5

Table 1: L27 Process parameters (Variables) and their varying levels

Sl. No.	Pulse ON Time (µs)	Pulse OFF Time (µs)	Current (Amp)	MRR (mm3/min)	Ra (µm)
1	20	9	3	5.62	0.35
2	20	9	4	6.54	0.30
3	20	9	5	6.95	0.62
4	20	12	3	6.35	0.27
5	20	12	4	6.48	0.29
6	20	12	5	6.59	0.35
7	20	15	3	5.80	0.11
8	20	15	4	6.58	0.10
9	20	15	5	6.35	0.49
10	35	9	3	6.65	0.54
11	35	9	4	7.21	0.65
12	35	9	5	7.86	0.55
13	35	12	3	6.50	0.30
14	35	12	4	6.31	0.48
15	35	12	5	7.01	0.55
16	35	15	3	6.35	0.15
17	35	15	4	6.21	0.42
18	35	15	5	6.90	0.62
19	50	9	3	7.62	0.75
20	50	9	4	7.49	0.65
21	50	9	5	7.84	0.98
22	50	12	3	7.45	0.60
23	50	12	4	7.20	0.55
24	50	12	5	7.56	0.75
25	50	15	3	6.32	0.29
26	50	15	4	7.21	0.55
27	50	15	5	7.82	0.50

Table 2: L27 Orthogonal Array and response.

ANOVA evaluation

ANOVA and regression analysis to analyze the outcomes of the tests, which were conducted with various cutting parameters (L27 array). The findings of the ANOVA evaluation for several cutting parameters are shown in Tabs. 3 and 4. The ANOVA study indicates that the statistical models offered can predict tool wear at a 95% confidence level. Finding the major variables affecting MRR and Ra values within 95% confidence was the goal of the experimental data analysis. For validation, normal probability graphs and main effect plots were employed. Terms were deemed insignificant and removed from the analysis if their p-value was less than 0.05. Tabs. 3 and 4 display the MRR and surface roughness (Ra) ANOVA results. The statistical models provided can forecast tool wear with a 95% confidence level, according to the ANOVA study. The objective of the analysis of the experimental data was to identify the primary influencing factors with 95% confidence. Main effect plots and normal probability graphs were plotted for validation [13]. Tab. 3 displays the ANOVA findings for the manufactured nano-MMCs' MRR. The "Pulse ON Time" metric contributes a significant percentage (47.01%) when compared with other factors like peak current & pulse off time, indicating that it is a very important component. "Pulse off time" was determined to be the least important component influencing the MRR of created nano composites. The surface roughness (Ra) ANOVA results for the fabricated nano MMCs are shown in Tab.

4. These results show that the "Pulse ON Time" has the biggest impact (36.64%) compared to the other factors, making it the most important parameter. "Pulse off time" and "peak current" are the next most significant factors influencing the surface roughness (Ra) values of the fabricated nano composites.

Sources	DoF	Seq. SS	Adj. SS	Adj. MS	F - Value	P - Value	% of Cont.	Remarks
p-on	1	4.7535	4.75347	4.75347	49.5105	0.0000004	47.01	Significant
p-off	1	0.9988	0.99876	0.99876	10.4027	0.0037449	09.89	Significant
A	1	2.1494	2.14936	2.14936	22.3869	0.0000909	21.26	Significant
Error	23	2.2082	2.20822	0.09601			21.84	
Total	26	10.1098					100	

Table 3: ANOVA response for MRR.

Sources	DoF	Seq. SS	Adj. SS	Adj. MS	F - Value	P - Value	% of Cont.	Remarks
p-on	1	0.41709	0.417089	0.417089	42.0089	0.0000013	36.64	Significant
p-off	1	0.25920	0.259200	0.259200	23.1064	0.0000356	22.77	Significant
A	1	0.23347	0.233472	0.233472	23.5152	0.0000678	20.51	Significant
Error	23	0.22836	0.228357	0.009923			20.06	
Total	26	1.13812					100	

Table 4: ANOVA response for Ra values.

Tabs. 5 and 6 display rankings for each attribute at different levels. Tab. 5 presents the average (mean) Material Removal Rate (MRR) values at different levels of the machining parameters pulse ON time, pulse OFF time, and current. The "Delta" number represents each parameter's impact on MRR by showing the difference among the highest and lowest values mean responses. According to the table, pulse ON time has the greatest impact on MRR, with the highest Delta value (1.028) and ranking 1. This indicates that material removal is greatly increased by increasing pulse ON time. Pulse OFF time had the least impact on MRR (rank 3), while current is ranked 2, indicating a modest contribution. Overall, the findings imply that pulse ON time and current are the main factors influencing MRR, with pulse OFF duration having little effect. The mean roughness of the surface (Ra) values at various machining settings for parameters are also displayed in Tab. 6. The degree to which each parameter affects surface roughness is shown by the Delta value. The findings show that the most significant component influencing surface roughness is pulse ON time, which has the largest Delta value (0.3044) and is rated 1. This suggests that increased pulse ON time raises Ra because of increased discharge energy as well as surface damage. Because of its function in spark stability and debris removal, pulse OFF time is graded 2, suggesting a moderate effect. With a ranking of 3, Current has less of an impact on Ra.

Levels	Pulse ON-Time (μs)	Pulse OFF-Time (μs)	Current (Amp)
1	6.362	7.087	6.518
2	6.778	6.828	6.803
3	7.390	6.616	7.209
Delta	1.028	0.471	0.691
Rank	1	3	2

Table 5: Mean response for MRR.

Levels	Pulse ON-Time (µs)	Pulse OFF-Time (µs)	Current (Amp)
1	0.3200	0.5989	0.3733
2	0.4733	0.4600	0.4433
3	0.6244	0.3589	0.6011
Delta	0.3044	0.2400	0.2278
Rank	1	2	3

Table 6: Mean response for Ra values.

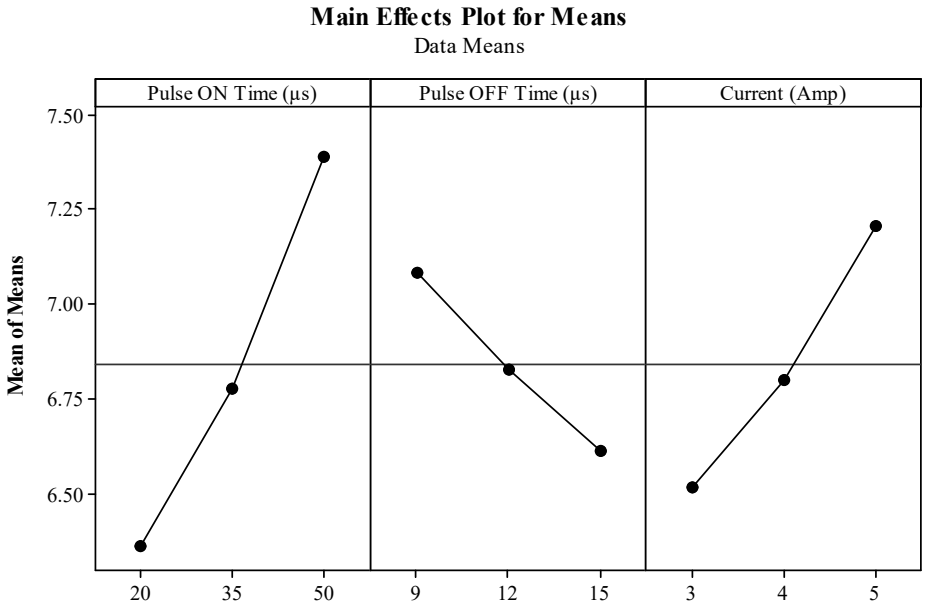

Figure 8: Main effect graph of MRR.

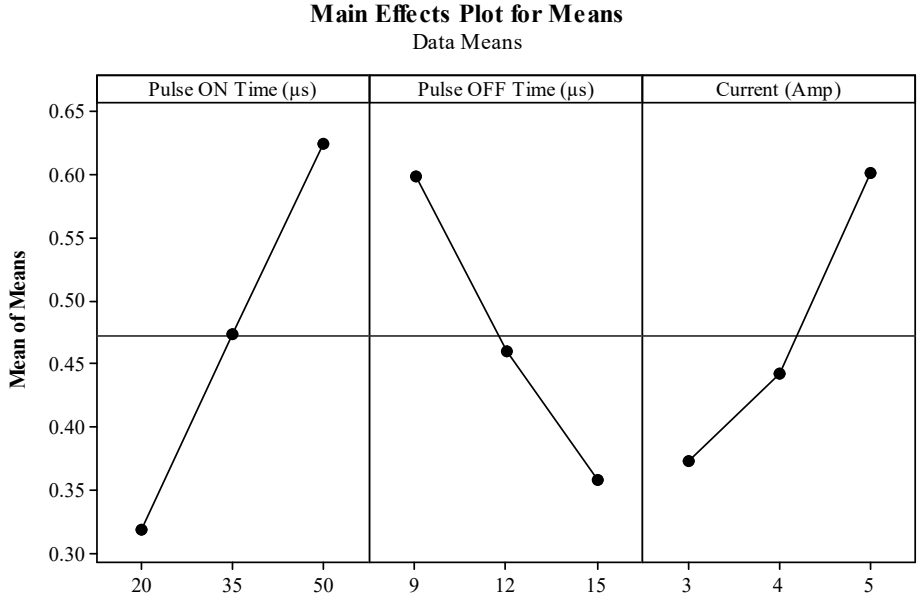

Figure 9: Main effect graph of Ra values.

The impact of specific machining parameters on the responses is demonstrated by the major effect plots for material removal rate (MRR) as well as surface roughness (Ra) in Figs. 8 and 9. Each parameter's levels are represented by the

horizontal axis in these plots, and the matching average response values are displayed on the vertical axis. Each line's slope represents a parameter's level of influence; a steeper slope denotes a greater effect, while a flatter line implies a smaller one. Because of the longer spark discharge duration, which produces more thermal energy and encourages more material melting and erosion, an increase in pulse ON time for MRR leads to a higher material removal rate [14On the other hand, even while debris removal as well as dielectric recovery are enhanced, increasing pulse OFF duration lowers MRR because longer intervals between subsequent discharges lower the effective spark energy and frequency input per unit time [15]. In a similar vein, MRR rises as current increases because higher current increases the discharge energy and removes more material per spark [16]. Because longer discharge times result in deeper and wider craters on the surface of the workpiece an increase in pulse ON time for surface roughness (Ra) results in a rougher surface finish [17]. On the other hand, longer pulse OFF times allow for greater debris flushing and dielectric medium stabilization, which produces craters that are more homogeneous and finer [15]. However, because high-energy sparks produce deeper craters, microcracks, and a finer surface texture, greater current levels typically result in increased surface roughness [18]. Overall, the findings show that while pulse OFF time helps to manage surface quality, pulse ON time and current have a considerable impact on both MRR and Ra.

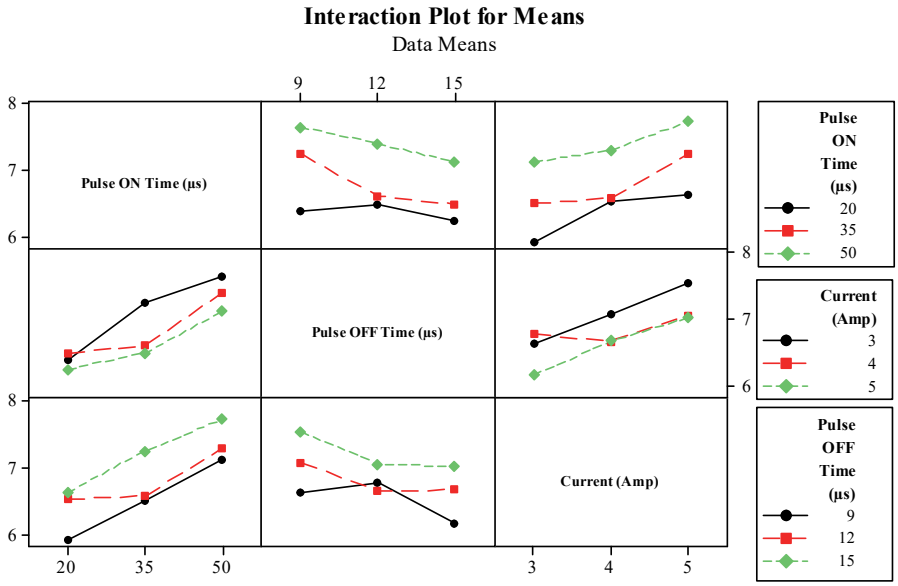

Figure 10: Interaction graph for the means of MRR.

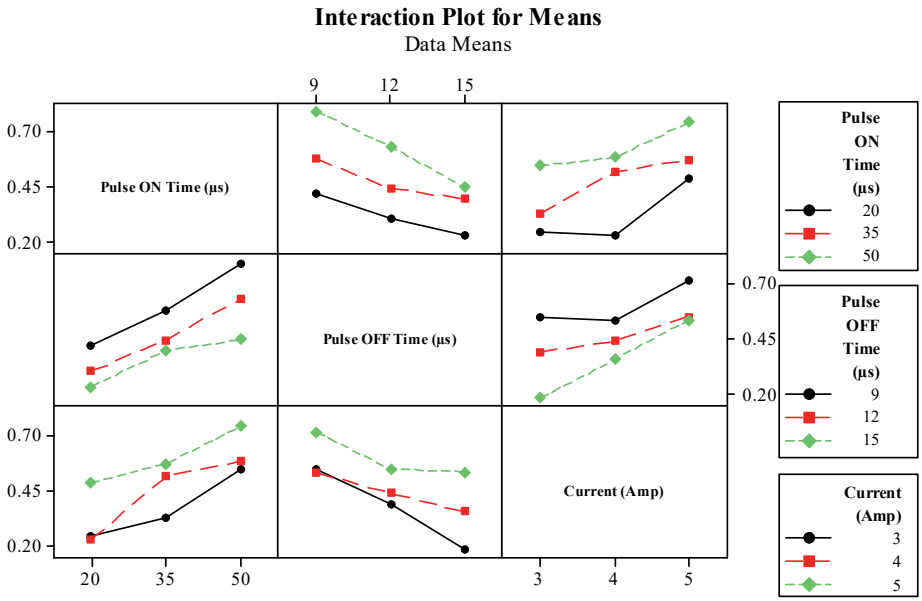

Figure 11: Interaction graph for the means of Ra values.

The interaction graphs that show how the parameters impact the evaluation of MRR and Ra values are shown in Figs. 10 and 11. In statistics and DOE (Design of Experiments), an interaction plot is a graphical tool used to show how the level of a second categorical factor affects the relationship between a continuous response variable and one factor. By showing how the quantity of one factor influences the response, an interaction plot also known as a statistical graph illustrates the relationship between two categorical factors and a continuous response variable [19]. When the lines on an interaction plot are not parallel, it indicates that the combined effects of the components are different from their individual effects. This is known as an interaction effect. The results show that there is a substantial interaction between the variables because the lines in these graphs overlap.

To determine the link between the responses and important process parameters, such as pulse ON time, pulse OFF time, and current (Amp), regression models were developed. Based on the significance of the factors found using ANOVA, regression equations were developed. The generated model's ability to predict both responses is confirmed by the validation investigation. The response achieved for both outputs is compared with experimental values obtained for the same set of parameters after the developed model has been modified to incorporate the expected sets of process variables. Eqns. 1 and 2 below provide the pertinent regression equations for each.

$$\mathrm{MRR}\left(\mathrm{mm}^3/\mathrm{min}\right) = 5.20426 + 0.0342593\,\mathrm{Pulse\ ON\ Time}\left(\mu\mathrm{s}\right) - 0.0785185\,\mathrm{Pulse\ OFF\ Time}\left(\mu\mathrm{s}\right) + \\ + 0.345556\,\mathrm{Current}\left(\mathrm{Amp}\right) \quad (1)$$

$$\mathrm{Ra}\left(\mu\mathrm{m}\right) = 0.141852 + 0.0101481\,\mathrm{Pulse\ ON\ Time}\left(\mu\mathrm{s}\right) - 0.04\,\mathrm{Pulse\ OFF\ Time}\left(\mu\mathrm{s}\right) + \\ + 0.113889\,\mathrm{Current}\left(\mathrm{Amp}\right) \quad (2)$$

In general, the responses within the parameters have been estimated using these equations (regression). Experiments have been conducted to verify the accuracy of the prediction values, and graphical comparisons between the experimental and predicted findings have been made. Figs. 12(a) and (b) compare the experimental and projected values for MRR and Ra, respectively. The figures show a significant correlation between the experimental and anticipated values.

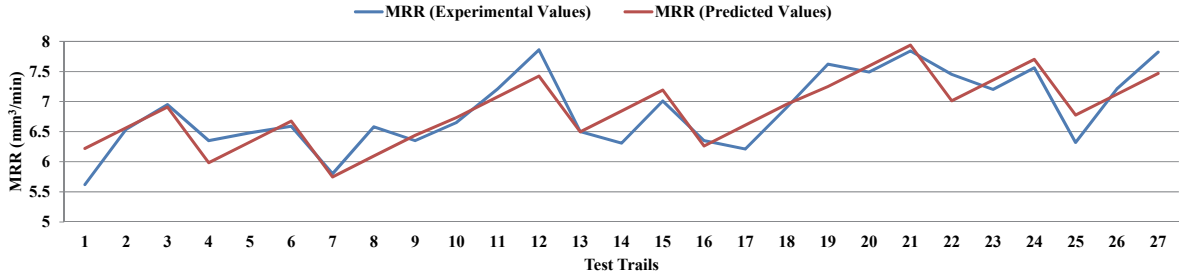

Figure 12(a): Comparison between Experimental and Predicted MRR Values.

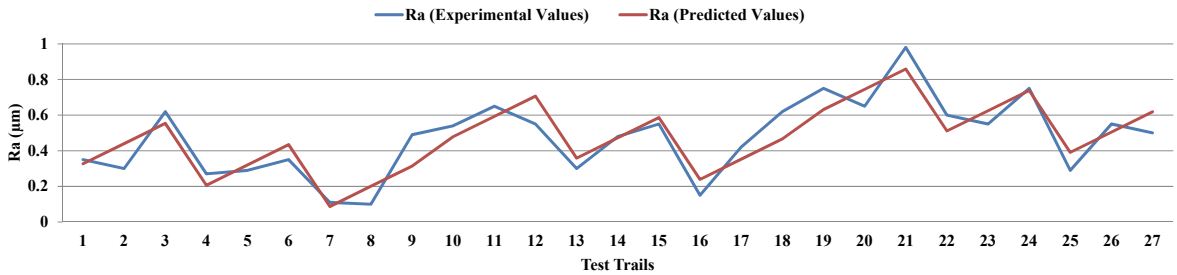

Figure 12(b): Comparison between Experimental and Predicted Ra Values.

A confirmation test was used to finalize the experimental design. The best parametric parameters recommended by the Taguchi method and the genetic algorithm were used in confirmation studies. The Main Effects Plot for Means within acceptable bounds was used to determine the ideal parameter levels. The fabricated nano-composites had a maximum variation of 8.33% for Ra and 3.82% for MRR, according to the confirmation test results. Tab. 7 displays the ideal parameter levels along with the matching findings of the confirmation test.

Characteristics	Pulse Time ON (μS)	Pulse Time OFF(μS)	Peak Current (A)	OA Exp. outcomes	Confirmatory Exp. outcomes	Error (%)
MRR (mm^3/min)	40	14	5	7.08	7.20	1.6
Ra (μm)	28	13	3	0.25	0.24	4.0

Table 7: Confirmatory test levels and outcomes of wear loss

CONCLUSIONS

The impact of n-TiC reinforcement on the mechanical and wear characteristics of Al7075 composites is examined in this research. Additionally, molybdenum wire electrodes were used in Wire Electrical Discharge Machining (WEDM) investigations on Al7075/n-TiC composites. These investigations led to the following conclusions:

- Al7075+n-TiC MMCs have been successfully produced by using stir-casting technique.
- The results show that the mechanical and tribological properties of Al7075 composites improve with increasing n-TiC content up to 3 wt. %, owing to uniform particle distribution, grain refinement, and enhanced load transfer. Beyond this level (at 4 wt.%), a decline in material properties is found due to high particle agglomeration, increased porosity and poor interfacial bonding, which adversely affects the strength and wear resistance. This optimal-reinforcement level (3 wt. %) was therefore selected for machining studies.
- Compared to un-reinforced alloy (Al7075), the mechanical, tribological, and wear properties were greatly improved by the addition of n-TiC; hardness, tensile strength, and wear resistance increased by 28.57%, 24.41%, and 33.69%, respectively.
- The Material Removal Rate (MRR) is improved by increasing pulse ON time and current because of the increased discharge energy. But by forming larger craters, these circumstances also make the surface rougher. Longer pulse OFF times, on the other hand, lower MRR while improving surface quality through improved dielectric recovery and debris flushing, leading to more consistent and stable machining conditions.
- The ANOVA results show that the "Pulse ON Time" has the biggest impact (47.01 %) on MRR and 36.64% impact on surface roughness values compared to the other factors such as “Pulse OFF Time and Peak Current (Amp).
- The results of the confirmatory test with a new set of experimental parameters. The obtained results, revealed a maximum of 1.6% error in MRR and 4.0% errors in the Ra values of the developed nano composites. This is within acceptable limit.

REFERENCES

[1] Ravikumar, M. (2025). Investigation on the tensile strength, hardness, and wear properties in n-B4C reinforced Al7075 composites, Fracture and Structural Integrity, 73, pp. 219-235. DOI: https://doi.org/10.3221/IGF-ESIS.73.15

[2] Shandilya, P., Jain, P.K. and Jain, N.K. (2012). Parametric optimization during wire electrical discharge machining using response surface methodology, Procedia Engineering, 38, pp. 2371-2377. DOI: https://doi.org/10.1016/j.proeng.2012.06.283

[3] Suhas, B. G., Chidanand, K. M., Kiran Kumar, K. U., Umesh, G. L. (2025). Study on mechanical and tribological characterization of titanium diboride (TiB2) reinforced Al7075 composites by Taguchi technique, Journal of Materials and Engineering Structures, 12, pp. 139-154.

[4] Kumar, A., Kumar, V., Kumar, J. (2013). Investigation of machining parameters and surface integrity in wire electric discharge machining of pure titanium, Proc. Inst. Mech. Eng. B J. Eng. Manuf., 227(7), pp. 972-992. DOI: https://doi.org/10.1177/0954405413479791

[5] Prakash, Gangadharappa, M. and Somashekar. (2024). Impact of nanoparticles (B4C-Al2O3) on mechanical, wear, fracture behavior and machining properties of formwork grade Al7075 composites, Fracture and Structural Integrity, 69, pp. 210-226. DOI: https://doi.org/10.3221/IGF-ESIS.69.15

[6] Amrish Raj and Senthilvelan. (2015). Empirical modeling and optimization of process parameters of machining titanium alloy by wire-EDM using RSM, Materials Today: Proceedings, 2(4-5), pp. 1682-1690.

DOI: https://doi.org/10.1016/j.matpr.2015.07.096
[7] Suchendra, K. R., Sreenivasa Reddy M., Mukundaiah, R. (2023). Influence of quenching agents on mechanical, wear, and fracture characteristics of Al2O3/MoS2 reinforced Al-6061 hybrid metal matrix composite (MMCs), Frattura ed Integrità Strutturale, 63, pp. 122-133. DOI: https://doi.org/10.3221/IGF-ESIS.63.12
[8] Samson Khalkho, J., Vidyasagar Chevuri, S. and Karunakar Dagarapu, B. (2023). Evaluation of microstructure and mechanical properties of TiO2 reinforced aluminium composites developed through multi-step stir casting, International Journal of Metalcasting, 17(1), pp. 272-283. DOI: https://doi.org/10.1007/s40962-022-00760-6.
[9] Hany S. Abdo, Asiful H. Seikh, Ahmed Fouly and Sameh A. Ragab. (2021). Synergistic strengthening effect of reinforcing spark plasma sintered Al-Zn-TiC nanocomposites with TiC nanoparticles, Crystals, 11, 842. DOI: https://doi.org/10.3390/cryst11080842.
[10] Ravikumar, M., Naik, R., Vinod, B. R., Chethana, K. Y., and Rammohan, Y. S., (2023). Study on nanosized Al2O3 and Al2O3-SiC on mechanical, wear and fracture surface of Al7075 composites for soil anchoring applications, Materials Physics and Mechanics, 51(6), pp. 24-41. DOI: https://doi.org/10.18149/MPM.5162023_3.
[11] Gowrishankar, T. P., Umesh, G. L., Vinod, B. R., and Ravikumar, M., (2025). Studies on mechanical, fractured surface, wear, and thermal characteristics of TiC reinforced structural grade Al6061 MMCs, Fracture and Structural Integrity, 74, pp. 373-384. DOI: https://doi.org/10.3221/IGF-ESIS.74.23
[12] Suresh Shivaramakrishna, R. and Raghavendra Subramanya. (2026). Influence of Fe3O4 particles in Al7075 metal matrix composites: a tribological study, Superficies y Vacio, 39, pp. 1-8. DOI: https://doi.org/10.47566/2026_syv39_1-260301
[13] Ravikumar, M., Suresh, R., Pruthvi, H. M., Prasad, C. D., Ramesha, H., Sudarshan, T. A., Varun, K. R., Masum, H., Kumar, C. H. (2025). Study on mechanical, tribological and fracture behaviour of n-Al2O3 reinforced Al7075 composites using Taguchi technique, International Journal of Cast Metals Research, 38(2-3), pp. 109-120. DOI: https://doi.org/10.1080/13640461.2025.2495509.
[14] Jithin and Suhas S. Joshi. (2021). Surface topography generation and simulation in electrical discharge texturing: a review, Journal of Materials Processing Technology, 298, 117297. DOI: https://doi.org/10.1016/j.jmatprotec.2021.117297.
[15] Kumar, S., Singh, R., Singh, T. P., Sethi, B. L. (2009). Surface modification by electrical discharge machining: a review, Journal of Materials Processing Technology, 209(8), pp. 3675-3687. DOI: https://doi.org/10.1016/j.jmatprotec.2008.09.032.
[16] Manjaiah, M., Laubscher, R. F., Kumar, A., Basavarajappa, S. (2016). Parametric optimization of MRR and surface roughness in wire electro discharge machining (WEDM) of D2 steel using Taguchi-based utility approach, International Journal of Mechanical and Materials Engineering, 11(7), pp. 1-9. DOI: https://doi.org/10.1186/s40712-016-0060-4.
[17] Khan, N. Z., Khan, Z. A., Siddiquee, A. N., Chanda, A. K. (2014). Investigations on the effect of wire EDM process parameters on surface integrity of HSLA: a multi-performance characteristics optimization, Production & Manufacturing Research, 2(1), pp. 501-518. DOI: https://doi.org/10.1080/21693277.2014.931261.
[18] Jai Prakash Agrawal, Nalin Somani and Nitin Kumar Gupta. (2026). Optimizing electric discharge machining parameters using Taguchi method and ANOVA: a study on AISI D2 steel machining with copper electrodes and materials science progress, Next Materials, 10, 101361. DOI: https://doi.org/10.1016/j.nxmate.2025.101361.
[19] Ganesh, K., Hemachandra Reddy, K., Sudhakar Babu, S., and Suresh, R., (2023). Investigation on microstructure, hardness, wear behavior and fracture surface analysis of strontium (Sr) and calcium (Ca) content A357 modified alloy by statistical technique, Frattura ed Integrità Strutturale, 65, pp. 32-46. DOI: https://doi.org/10.3221/IGF-ESIS.65.03.